Journal of Alloys and Compounds 508 (2010) 599–605

Contents lists available at ScienceDirect

Journal of Alloys and Compounds

journal homepage: www.elsevier.com/locate/jallcom

Photoinduced effects in TiO_2 nanocrystalline films with different morphology

Yahia Djaoued[a], K. Ozga[c], A. Wojciechowski[b], A.H. Reshak[d,e], J. Robichaud[a], I.V. Kityk[b,*]

[a] Laboratoire de Micro-spectroscopies Raman et FTIR, Université de Moncton-Campus de Shippagan, 218, boul. J.-D. Gauthier, Shippagan, NB, Canada E8S 1P6
[b] Electrical Engineering Department, Czestochowa University of Technology, Armii Krajowej Av. 17/19, Czestochowa, Poland
[c] Chair of Public Health, Czestochowa University of Technology, Armii Krajowej Av. 36B, 42-200 Czestochowa, Poland
[d] Institute of Physical Biology-South Bohemia University, Nove Hrady 37333, Czech Republic
[e] School of Microelectronic Engineering, University Malaysia Perlis (UniMAP), Block A, Kompleks Pusat Pengajian, 02600 Arau Jejawi, Perlis, Malaysia

ARTICLE INFO

Article history:
Received 21 July 2010
Received in revised form 18 August 2010
Accepted 26 August 2010

Keywords:
Photoinduced
TiO_2
Nanocrystalline films
Second harmonic generation
Third harmonic generation

ABSTRACT

The complex studies of photoinduced absorption, second harmonic generation and third harmonic generation were performed for TiO_2 films of different morphology. In particular we have studied the influence of a bicolor laser beam treatment by a 300 mW green cw laser emitting at 532 nm on changes of absorption, birefringence and third harmonic generation on TiO_2 films. We have performed the corresponding measurements using as a photoinducing light a glass erbium 10 ns pulsed laser with a fundamental wavelength of about 1540 nm together with its second harmonic generation (SHG) at 770 nm using the method of bicolor laser treatment and a frequency repetition of about 10 Hz. Varying the power density ratios between the fundamental and its SHG we have established the optimal conditions to achieve maximal photoinduced changes of absorption, birefringence and third harmonic generation (THG). We have detected changes of the birefringence and of the THG immediately after the laser treatment. We study an influence of the nanoparticle's sizes on the observed changes of the optical features. Additionally we have studied the role of different chemical treatment on the structural and optical parameters.

© 2010 Elsevier B.V. All rights reserved.

1. Introduction

During the last decade, basic and applied research focused on the preparation and characterization of TiO_2 thin films, possessing large energy gap, excellent visible and near-IR transmittance, high refractive index (2.2–2.75 in the visible spectral range) and dielectric constant (within the 120–190) [1–3]. It was found that TiO_2 is antibacterial, self-cleaning, super-hydrophilic, and able to decompose organic substances. Various other applications of TiO_2 thin films are encountered in electronics, optics, environment protection, and medicine. At the same time TiO_2 films present an important class of optoelectronic materials transparent in the visible and infrared (IR) region of the spectrum [4,27].

Besides they have high photosensitivity making them very interesting for integrated optical devices. Dozens of TiO_2 based materials, have been thus widely used in photovoltaic devices, optical gratings, waveguides, fibre and planar optical devices, optical sensors, optical circuits, holography, light amplifiers and generators [5], etc. Especial interest exists for their optically induced optical properties, particularly the nonlinear optical ones for applications in all-optics treatments. The TiO_2 nanocrystallites can play an important role in devices operated by coherent laser beams.

Up to this date, most of the photoinduced effects in films were performed using amorphous as well as partially crystallized chalcogenides both in glass form, and the origin of the effects were determined by the changes of the linear and nonlinear optical constants [6,7]. These effects are a bit similar to those observed in metallic nanoparticles [8], however, for an improved control of the process it would be better to have semiconducting nanoparticles with defined nanocrystallite sizes. TiO_2 nanocrystlallites deposited on different substrates are the perfect candidates for this role. Their photodarkening can be explained within a framework of several models and one of the most probable is a percollative growth of photodarkened local sites after illumination by photon-stimulated site switching, repulsion and slip motion of structural clusters [9]. For comparison, for silver-doped chalcogenides, the aggregation of Ag^+ ions in the illuminated region is the principal mechanism determining phototransparency changes [10], which means a limitation of the photoinduced changes due to the absence of effective photoinduced charge transfer between the substrate and the nano-trapping levels. IR stimulated changes contain two principal contributions: the photo-transient part, which disappears immediately after the switching-off of the laser irradiation, and the long-time relaxed "metastable" part persisting during a relatively long time at room temperature. Traditionally, the metastable contribution is erased after thermal annealing

* Corresponding author.
E-mail addresses: iwank74@wp.pl, ikityk@el.pcz.czest.pl, iwank74@gmail.com (I.V. Kityk).

0925-8388/$ – see front matter © 2010 Elsevier B.V. All rights reserved.
doi:10.1016/j.jallcom.2010.08.135

at a temperature determined by the glass transition temperature.

The TiO_2 films, in the form of nanocrystallites, may be considered as a serious competition to the amorphous chalcogenide films due to the specific origin of the prevailingly 2pO–3dTi ionic valence bonds and the relatively flat conduction bands. These films have a substantial advantage with respect to other semiconductors due to the possibility of occurrence in them of nonlinear optical effects and, due to their high photosensitivity, which may be promising for different photovoltaic devices [11]. Moreover, the absorption edge of bulk anatase (TiO_2) crystal around 3.2 eV is associated with indirect optical band gap transitions. Additionally, widening of the band gap might be expected in nanosized materials [12], so the phonon subsystem may play here also an important role. Indeed, it is shown that decreasing the diameter of the spherical nanoparticles in anatase TiO_2 by 10 nm is accompanied by a band gap variation within 0.2–0.4 eV [13]. Besides the indirect band gap transition mentioned above, a transition at about 3.8 eV has been ascribed to the direct optical band gap in different anatase TiO_2 films [14]. Few direct inter-band transitions with an energy higher than 3.8 eV are also predicted [15,16]. In such kind of nanocrystalline semiconductors the relatively flat bands possessing both properties of delocalized long-range ordered bands and localized states originating from the nanoconfinement effects begin to play a principal role [17]. Also, in the case of TiO_2 amorphous films, the ellipsometrically measured pseudodielectric function spectra have shown three distinct structures at about 3.3, 3.9 and 4.9 eV, which have been assigned to the transitions at the principal van Howe points in the Brillouin zone.

It is crucial to control the synthesis in order to develop an expected material of moderate cost and flexible properties. The use of TiO_2 films with controlled nanocrystalline sizes may open a new step in materials for recording and transformation of optical information and for optical switching. In particular, such nanocrystalline materials may be promising for nonlinear optical effects [18]. For this investigation we have synthesized anatase TiO_2 nanocrystalline films of different sizes with different chemical treatments. In Section 2 are presented the principal parameters of film growth and their structural and morphology monitoring methods. Section 3 presents the principal parameters of the synthesized films and discuss the relation between the film sizes/structure and the photoinduced changes observed.

2. Experimental methodology

2.1. TiO_2 films preparation

Titanium tetra-*n*-butoxide (TTB) obtained from Aldrich Chem Co. was used as the starting material in the preparation the TiO_2 films. The concentration of TTB in the solution was 0.5 mol/L. TTB was first mixed with a small amount of ethanol in a container and stirred for 30 min. A mixture of water containing 3 wt.% HCl and ethanol was poured under stirring into the transparent solution to promote hydrolysis; the molar ratio of H_2O to TTB was 1:1. Finally, poly-ethylene glycol of molecular weight ~600 (PEG 600) was added slowly to this solution and stirred for 1 h. The resulting solution was used for the TiO_2 film coating. The molar ratio of PEG to TTB was 1. Films annealed at 400 °C and below were coated on corning glass substrates, whereas films annealed at temperatures from 500 to 900 °C were deposited on vitreous silica. A dipping solution was also prepared without PEG and used for coating. A custom-built dip-coating apparatus was used for the depositions. The substrate was lowered into the coating solution for 30 s and then withdrawn at a regulated speed of 4 mm/s. After each coating, the films were first dried at 60 °C for 2 min and then heat treated at 90 °C for 1 h in air inside an oven. These samples were then treated in hot water at 90 °C for 1 h. Thereafter, the films were heated at a rate of 0.5 °C to annealing temperatures ranging between 100 and 700 °C. The samples were held at the peak temperature for 1 h and then cooled to room temperature. A thin film prepared in presence of PEG 600 and treated in hot water alone was denoted as sample C1. The thin films prepared in presence of PEG, treated in hot water and heated in air at temperatures of 100–700 °C, were denoted as samples C2–C8. Three samples, prepared without PEG, treated in hot water and thereafter heat treated at temperatures of 500, 600, and 700 °C, were denoted as samples C11, C12, and C13.

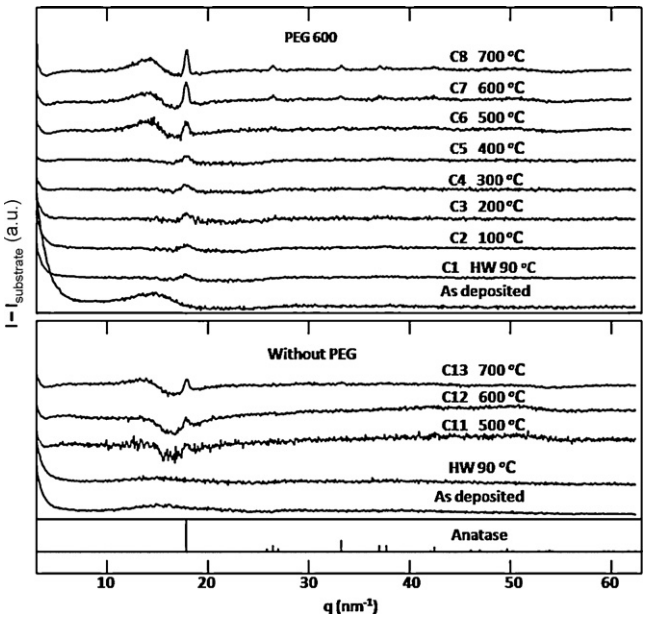

Fig. 1. X-ray scattering intensities of the TiO_2 films prepared in presence of PEG 600 as a function of the scattering vector (top portion) and of those prepared without PEG (bottom portion). The scattering originating from an empty substrate was subtracted. The films were annealed at the indicated temperature. The powder scattering intensities for anatase are shown at the bottom of the diagram.

2.2. TiO_2 films characterization

X-ray diffraction measurements were carried out with a custom-built diffractometer equipped with graphite monochromator and analyzer crystals. The data were taken in reflection mode with Cu Kα radiation (λ = 0.1542 nm), and the signal measured from the glass and quartz substrates was subtracted from the data. The crystalline phases were identified using the ICDD/JCPDS database [Powder Diffraction File, ICDD, JCPDS, Swarthmore, PA, 1988 (Card Nos. 21-1272, 21-1276 and 29-1360)]. Crystal sizes were determined based on the anatase (1 0 1) and (2 0 0) peaks using the Scherrer formula [19].

Raman spectra were recorded at room temperature with a Jobin-Yvon Labram HR microanalytical spectrometer equipped with a motorized *xy* stage and autofocus. The spectra were generated with a 17 mW, 632.8 nm He–Ne laser excitation and were dispersed with the 1800 g/mm grating across the 0.8 m length of the spectrograph. The laser power was 9 mW on the sample surface. The spectral resolution of this apparatus is estimated to be less than 0.5 cm^{-1} for a slit width of 150 μm and a confocal hole of 300 μm.

Scanning electron microscope (SEM) images were recorded for the films before and after hot water treatment at 90 °C, using a JEOL JSM-5600 SEM (JEOL USA, Peabody, MA). The microscope was operated at 10 kV, at a working distance of 10–15 mm, and with a 45° specimen tilt.

Transmission electron microscopy (TEM) of a powder sample was performed by placing a small amount of the sample into a glass vial. Ethanol was added and the solution was sonicated for 10 min. A drop of the solution was placed onto a carbon coated 200 mesh copper grid and left to dry overnight. The sample was imaged using a 2011 JEOL STEM at 200 keV. Images were captured on a 4 k × 4 k multiscan CCD camera using Digital Micrograph from Gatan.

For the band gap measurements, the transmission spectra of the films were recorded at normal incidence with a Biochrom Ultrospec 2000 UV–Visible spectrophotometer.

2.3. Optical measurements

Optical spectra were measured by spectrophotometer with a resolution of about 1.5 nm. We also have performed the photoinduced measurements using as a photoinducing light a glass erbium 10 ns pulsed laser with a fundamental wavelength of about 1540 nm together with its second harmonic generation at 770 nm (so-called writing beam) using the method of bicolor laser treatment [20] at a frequency repetition of about 10 Hz. Varying the power density ratios between the fundamental and the writing beams, we have established the optimal conditions to achieve the maximal photoinduced changes, both linear as well as nonlinear. We have detected changes of the birefringence and of the third harmonic generation during, and immediately after the cw 532 nm laser treatments at a power of about 300 mW. The photoinducing beam possessed a Gaussian-like beam profile. The Senarmont

Table 1
Particle sizes as determined by XRD and Raman micro spectroscopy, and indirect and direct optical band gaps of the anatase TiO_2 nanocristalline films.

	Treatment temperature (°C)	Size from XRD (nm)	Size from Raman (nm)	Indirect band gap E_g (eV)	Direct band gap E_g (eV)
Sample obtained from TiO_2 solution containing PEG 600					
C1	90	4.8	5.5	3.31	3.81
C2	100	4.8	5.5	3.52	3.86
C3	200	6.5	5.5	3.51	3.85
C4	300	5.6	5.6	3.51	3.85
C5	400	6.8	5.8	3.49	3.85
C6	500	10	9.7	3.45	3.70
C7	600	12	14	3.43	3.69
C8	700	16	16	3.45	3.72
Sample obtained from TiO_2 solution without PEG					
C11	500	12	9.4	3.51	3.94
C12	600	9.0	11	3.51	3.91
C13	700	13	14	3.51	3.91

method for the cw 4 mW He–Ne laser was used for detection of the birefringence changes. Generally, the procedure was similar to the one used for the observations performed in Ref. [21].

3. Results and discussion

3.1. XRD study on the TiO_2 nanocrystalline films

Fig. 1 shows the XRD data of the TiO_2 films prepared in presence of PEG 600 (top portion) and of those prepared without PEG (bottom portion). The as-deposited films scatter X-rays below 5 nm^{-1}, as well as between 11 and 18 nm^{-1}. For the films prepared in presence of PEG 600, treatment in hot water at 90 °C for 1 h (sample C1) eliminates most of the diffuse scattering, and leads to an anatase crystalline phase. Annealing after treatment in hot water leads to a sharper anatase (1 0 1) peak at 17.85 nm^{-1}. The anatase (2 0 0) peak at 33.21 nm^{-1} is the second prominent peak of this phase. Table 1 presents the crystallite sizes of the films for different treatment temperatures as determined from the Scherrer formula. After treatment in hot water at 90 °C, the crystallite size is ~5 nm for samples prepared with PEG 600. Upon annealing at 500 °C, the crystallite size increases to 10 nm. The crystallite size increases to ~16 nm as the annealing temperature is raised to 700 °C.

The samples prepared without PEG show no sign of crystallization after the hot water treatment, and show anatase crystals after annealing at 500 °C in air for 1 h.

3.2. Micro-Raman study on the TiO_2 nanocrystalline films

Fig. 2 shows the Raman spectra of films obtained from a TiO_2 solution prepared in presence of PEG 600 (left portion) and without PEG (right portion). The spectra of the films prepared in presence of PEG 600 show the crystallization of the film after a hot water treatment at 90 °C, as evidenced by the presence of the characteristic anatase Raman modes at ~150, 404, 518 and 637 cm^{-1}. The main anatase Raman band is very broadened (32.1 cm^{-1}) and high-frequency shifted (~150 cm^{-1}) as compared to the Raman spectrum of commercial anatase TiO_2 powder (Aldrich) which has the peak position (PP) at 142.5 cm^{-1} and a full width at half maximum (FWHM) of 7.5 cm^{-1}. These features present the main aspect of nanocrystalline TiO_2 [22]. Using a phonon confinement model; it is possible to obtain an estimate of the crystallite size from the

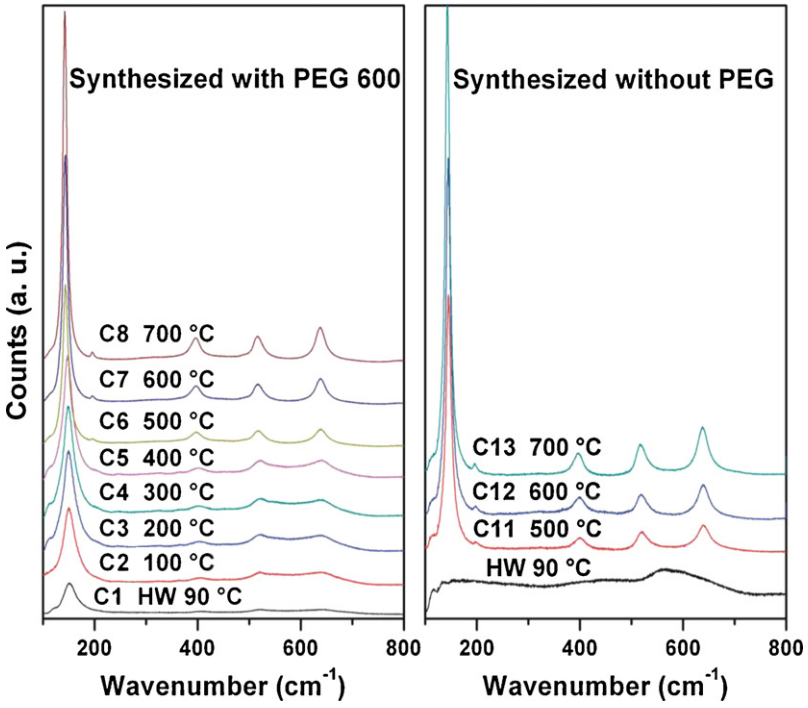

Fig. 2. Raman spectra as a function of treatment temperature of the TiO_2 films obtained from a solution prepared in presence of PEG 600 (left portion) and without PEG (right portion).

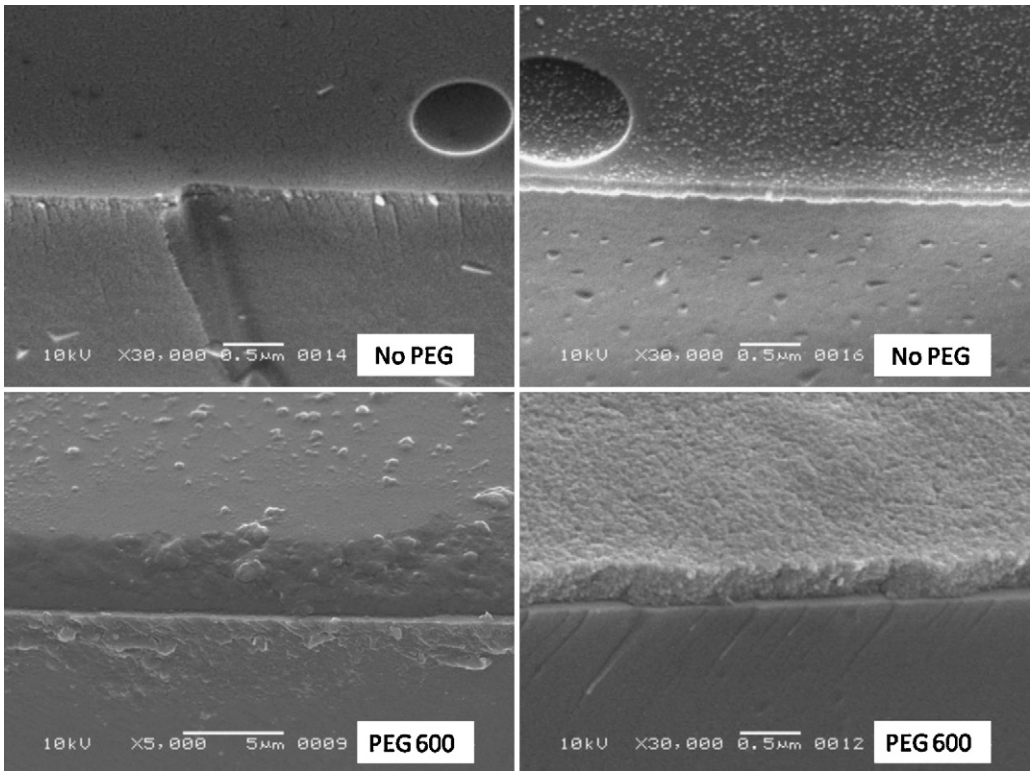

Fig. 3. SEM images of the TiO_2 films prepared from solutions having no PEG (top images) and PEG of molecular weight 600 (bottom images), before the hot water treatment (left images), and after the hot water treatment (right images).

FWHM and the position of the anatase main Raman peak. The thus estimated crystallite sizes are shown in Table 1. We attribute the large shifts and broadening of the main Raman band of the anatase phase mainly to the particle quantum size effect [23]. Upon annealing, and with an increase in the annealing temperature, the crystallite tend to agglomerate and grow in size, thus the frequency and width of the peaks tend towards those of the commercial anatase TiO_2 powder. Upon annealing the films at 500 °C, the crystallite size increased to 10 nm for the sample prepared with PEG 600 (sample C6).

The rightmost portion of Fig. 2 shows the Raman spectra of samples prepared from a PEG-free dipping solution treated at 90 °C in hot water, and then further annealed at temperatures of 500, 600, and 700 °C. The Raman spectrum of the hot water treated film shows no sign of crystallization, and further annealing of the hot water treated films (annealing from 100 to 400 °C not shown here) showed that the crystalline features of anatase TiO_2 only appeared at 400 °C, and that further annealing at 500 °C was necessary for complete crystallization to take place. This confirmed the role of PEG in the low temperature crystallization of TiO_2 films.

3.3. SEM study on the TiO_2 nanocrystalline films

Fig. 3 shows SEM images of the films prepared from solutions having no PEG (top images) and PEG of molecular weight 600 (bottom images). The films have a 45° tilt in order to show the surface features. The images on the left and right show the microstructure of the films before and after hot water treatment for 1 h, respectively. Before the hot water treatment (left images) the film surfaces are smooth and it can be seen that the thickness of the film containing PEG 600 (bottom left) is high (~4.9 μm). After the hot water treatment (right images), the PEG containing film was crystallized (sample C1) while the film with no PEG remained amorphous. For the PEG containing film, after the hot water treatment, the cross section of the film is rough, due to the formation of anatase nanocrystals, not only on the surface but also inside the film. The thickness of the film is also much decreased (down to 0.4 μm), attributed to the removal of PEG. The removal of PEG has also resulted in a porous structure. Contrary to the PEG containing film, the thickness and surface roughness of the film without PEG did not change significantly (top images).

3.4. TEM study

A TiO_2 powder was prepared from a sol containing PEG 600, similar to the one used for the TiO_2 thin films preparation. The sol was aged for several days and dried in air at a temperature less than 90 °C until a white powder was obtained. This powder was subsequently treated in hot water at 90 °C for 1 h in order to remove the PEG and to get crystalline TiO_2 in the anatase form. The anatase TiO_2 nature of the powder was confirmed by Raman microscopy.

Fig. 4 shows TEM images of the obtained TiO_2 powder. The particle size is estimated to be around 5–6 nm with nanometer sized interparticle distances thus exhibiting microporous features. This particle size is slightly higher than the reported size for the thin film particles (4.8 nm). The size difference is confirmed by Raman since the powder presents a FWHM of 34 cm^{-1} as compared to 39 cm^{-1} for the thin film.

3.5. Photo absorption of the TiO_2 nanocrystalline films

The optical band gaps of the films were determined from the UV–Visible transmission spectra using the relation:

$$\alpha h\nu = A(h\nu - E_g)^n \quad (1)$$

where α is the absorption coefficient, A is a constant and E_g is the optical band gap of the film [24]. For the anatase polymorph of TiO_2, the optical transition is indirect, and $n = 2$ in Eq. (1). In the region of

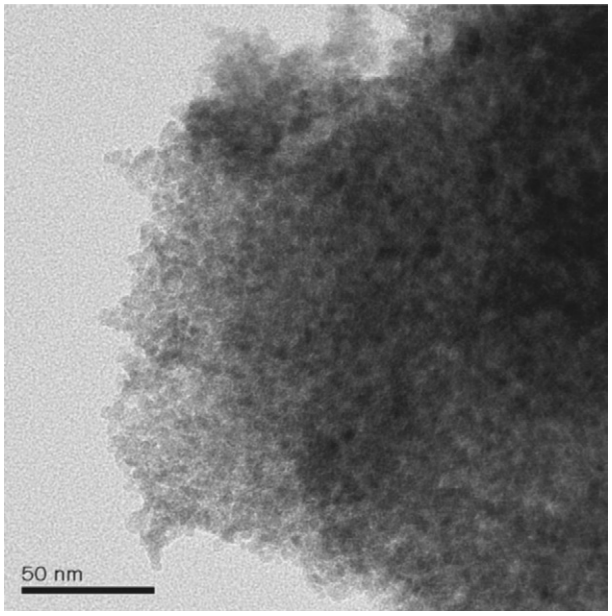

Fig. 4. TEM image of a TiO_2 powder prepared from a sol containing PEG 600 similar to the one used for the TiO_2 thin films preparation and treated in hot water at 90 °C for 1 h.

strong absorption, and at normal incidence, the reflectivity is very small and can be neglected [25]. This leads to the following expression for the absorption coefficient α as a function of transmittance T:

$$\alpha = \frac{-2.303 \log T}{t} \quad (2)$$

where t is the film thickness [25]. The reflectivity is relatively low and may be ignored. Eq. (1) then becomes $-2.303h\nu \log T = B(h\nu - E_g)^2$, and the graph of $(-2.303h\nu \log T)^{1/2}$ versus $h\nu$ will present a linear part that can be extrapolated to zero, leading to E_g. Here coefficient B corresponds to the coefficient of the absorption edge. The direct optical band gap of the films was also determined by using $n = 1/2$ in Eq. (1). The optical band gaps of the anatase TiO_2 nanocristalline films are presented in Table 1.

In Fig. 5 are presented typical absorption spectra of the studied TiO_2 nanocrystalline films. There occur some spectral peaks formed partially by the interference observed at 420, 440, and around 650 nm.

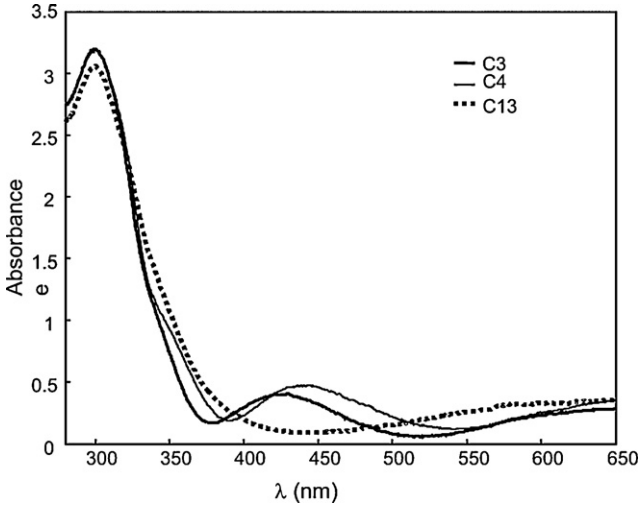

Fig. 5. Typical absorption spectra of the TiO_2 films with different nanocrystallite sizes.

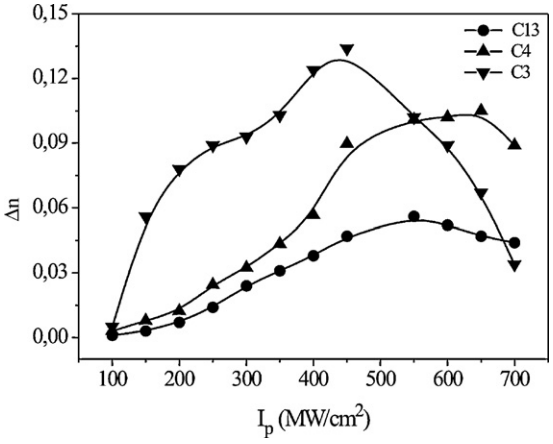

Fig. 6. Photoinduced changes of the birefringence ($\times 10^{-2}$) for the cw He–Ne 1150 nm wavelength. The photoinduction was performed by bicolor laser beams at 1540 and 740 nm taken in the ratio 8:1.

The ellipsometric study has shown that the roughness of the samples was evaluated to be 6.54 nm.

Due to charge transfer between the 2pO–3dTi chemical bonds and also due to their exceptional photosensitivity, in the present work we explore the influence of bicolor (1540 nm/770 nm) laser beam treatment, as well as a treatment by a 300 mW green cw laser emitting at 532 nm to form photoinduced changes of optical constants.

In Fig. 6 are presented the behavior of birefringence after 3–5 min of bicolor optical treatment and during the optical treatment by the green laser. The green cw laser was unpolarized and the bicolor treatment was polarized with a degree of polarization not higher than 30%. To exclude any non-accuracies related to the sample's non-homogeneities we have done the studies at different points of the samples. From Fig. 6 one can see that the maximal changes of the birefringence were achieved for sample C3 (up to 0.13×10^{-2}) possessing average NP sizes of about 6.0 nm. The maximum of the photoinduced birefringence was observed at a power density equal to about 450 MW/cm^2, and further increase of the photoinducing laser beam power density leads to faster decrease of the corresponding birefringence. For sample C4 (average sizes 5.6 nm) this maximum was observed for higher bicolor laser power densities (about 640 MW/cm^2) and the maximally achieved birefringence was equal to about 0.10×10^{-2}. Substantially less effect was observed for sample C13 (average sizes 13.5 nm) with the maximum equal to about 550 MW/cm^2. We limit our presentations only to samples C3, C4, and C13, because for the other samples the features are similar.

The photoinduced birefringence effect exists only during cw laser treatment and substantially decrease after the interruption of the optical treatment. In turn, without the bicolor treatment, no birefringence is observed.

The local photothermal temperature changes did not exceed 20 K. At the same time, the use of a non-polarized photoinduced laser do not bring any changes. The effect is substantially different during bicolor treatment under the same conditions with simultaneous illumination by the same bicolor laser and a blue 405 nm laser operating at 300 mW. From Fig. 7, one can see that the maximum of the birefringence changes is larger for the C4 and C3 samples (with lower NP sizes) and, that for the larger NP sized C13 sample, the pump power features are only slightly disturbed. Moreover, the features are almost symmetrical with respect to the power densities.

The occurrence of the phenomenon after a power density higher than 400 mW/cm^2 may indicate that we deal with the re-charged

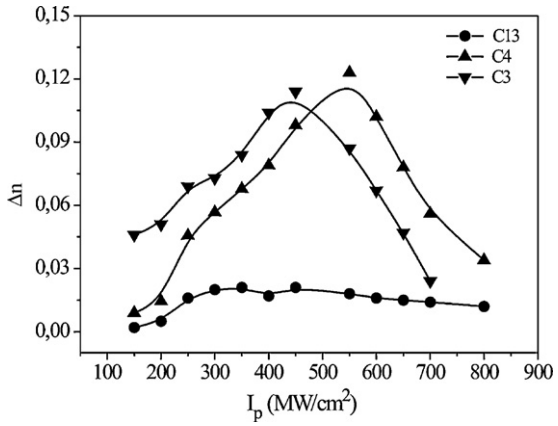

Fig. 7. The same as in Fig. 6 for the illumination by the second harmonic generation of the 1064 nm and its second harmonic generation at ratio 6:1.

interface trapping levels including those of nano-confined sheet origin. The birefringence during treatment by the two bicolor laser beams indicates that we deal with photopolarized states which are very sensitive to bicolor optical treatment. At the same time we have not observed an occurrence of photoinduced deformation using a dilatometric method. The space non-homogeneity of the photoinducing spot is below 15%. The measured changes have covered at least 75% of the irradiated surfaces. The reversible changes do not exceed 3%.

To explore the role of the cw green laser treatment, we have performed studies of the THG at 1540 nm pulsed laser fundamental beams. From Fig. 8, one can see that all the third harmonic generation (THG) signals decrease during the first 60 s of the cw laser treatment, and that it increases afterwards. One can see that the maximal signal is observed for the C3 sample and that for the C4 and C13 samples these values are less. However, the decrease of the THG signals is substantially higher. To understand the origin of this effect we have performed studies of photoinduced absorption changes (see Fig. 9). Following the dependences presented one can conclude that: for sample C3 there occurs additional spectral maxima situated at 335 nm and 410 nm (see Fig. 9a). The measurements were done for different times of treatment and it was established that after just 2 min, the spectra are almost saturated and that afterwards, the changes are not so obvious. The further switching-off of the cw laser treatment leads to a slow decrease of the maxima and only after 21 h these changes are more prominent. The observed maxima are caused by photoinduced polarization of the corresponding trapping levels below the energy gap and it may indicate the occurrence of additional effective optical oscillators

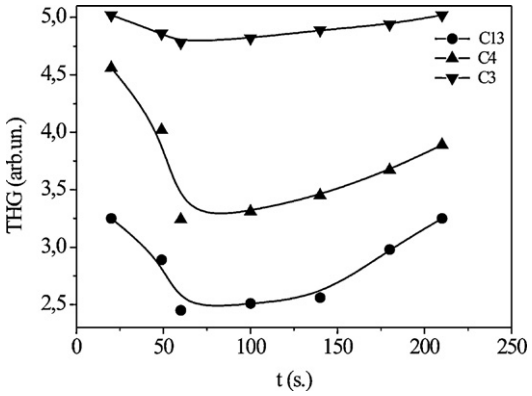

Fig. 8. Dependence of the THG versus the cw laser treatment.

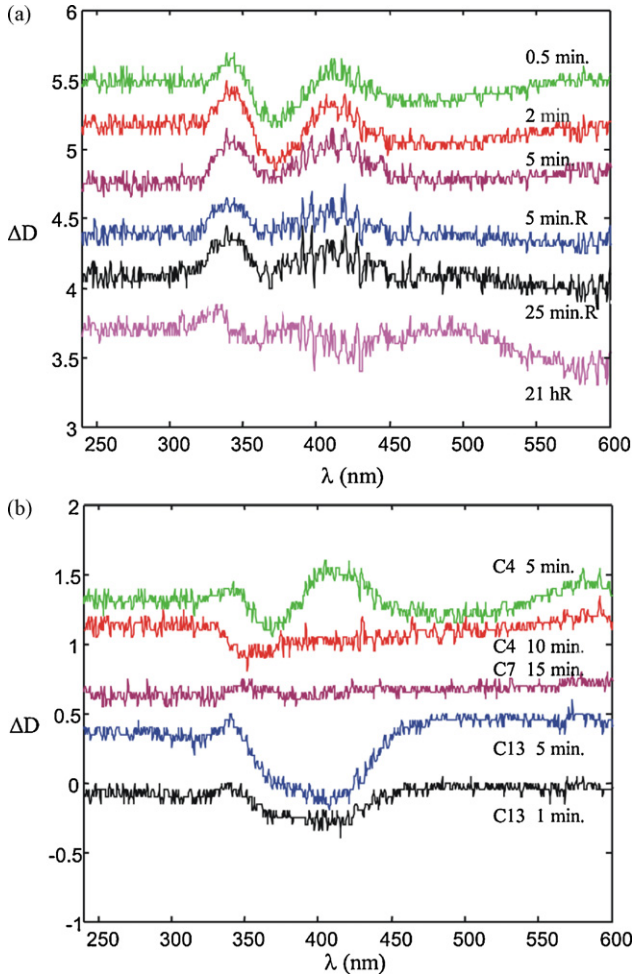

Fig. 9. (a) Photoinduced changes of absorption for sample C3 at different times of optical treatment and after the relaxation (R); (b) The photoinduced changes of the absorption for samples C4, C7 and C13 at different times of optical treatment.

contributing to the effect. Such slow relaxation may be caused by depopulation of the corresponding metastable levels.

From Fig. 9b, one can see that the photoinduced resonance maxima occurred at 335 and 406 nm. However, the figure shows a clear dependence on time of the cw laser treatment and that, for example, sample C4 shows a disappearance of the maxima after 10 min of treatment. Similarly, for sample C13 the maximum at 320 nm decreases and the minima at 380–410 nm also decrease after 1 min of treatment. It is crucial that the C7 sample (sizes about 13.0 nm) did not show any changes even after 15 min of treatment. Because the samples C7 and C13 have almost the same sizes (13.0 and 13.5 nm) such difference is caused by PEG treatment.

Finally it is necessary to emphasize that our attempt to see some SHG during bicolor laser treatment did not give any reliable signal. The observed differences between the THG and the SHG are caused by absence of the specific features of the photoinduced gratings. In this case we have the grating which is not non-centrosymmetric, but only centrosymmetric. As a consequence the effects described by the fourth rank tensors may be observed.

At the same time the birefringence was absent only during the cw laser treatment. In turn the THG was absent for the cw laser treatment. This is an additional confirmation that different mechanisms are determining the properties of the observed photoinduced effects.

To exclude contribution of the multi-photon excitations we have performed additional exploration of the multi-photon excitations,

in particular TPA. The contribution to the observed effect did not exceed 2%.

4. Conclusions

We explored the influence of a bicolor laser beam treatment (1540 nm/770 nm) and of a 300 mW green cw laser emitting at 532 nm on the photoabsorption, birefringence and THG of nanocrystalline TiO_2 films with different sizes and PEG treatment. Varying the power density ratios between the fundamental and the writing beams, we have established the optimal conditions to achieve maximal photoinduced changes, both linear as well as nonlinear. We have detected changes of the birefringence and of the THG, during, and immediately after the cw 532 nm laser treatment at a power of about 300 mW. The green cw laser was unpolarized and the bicolor treatment was polarized with a degree of polarization not higher than 30%. It was shown that the maximal changes of the birefringence were achieved for sample C3 (up to 0.13×10^{-2}) possessing average NP sizes of about 6.0 nm. The maximum of the photoinduced birefringence was observed at a power density equal to about 450 MW/cm^2, and further increase of the photoinducing laser beam power density lead to faster decrease of the corresponding birefringence. For sample C4 (average sizes 5.6 nm) this maximum was observed for higher bicolor laser power densities (about 640 MW/cm^2) and the maximally achieved birefringence was equal to about 0.10×10^{-2}. Substantially less effect was observed for sample C13 (average sizes 13.5 nm) with the maximum equal to about 550 MW/cm^2. For sample C7 the effect was not observed.

To explore the role of the cw green laser treatment, we have performed studies of the THG at 1540 nm pulsed laser fundamental beams. We have established that all the third harmonic generation (THG) signals decrease during the first 60 s of the cw laser treatment, and that it increases afterwards. The maximal signal is observed for the C3 sample. And for the C4 and C13 samples these values are less, however the decrease of the THG signals is substantially higher. To understand the origin of this effect we have performed studies of photoinduced absorption changes. Following the dependences presented one can conclude that: for sample C3 there occurs additional spectral maxima situated at 335 and 410 nm. The measurements were done for different times of treatment and it was established that after just 2 min the spectra are almost saturated and that afterwards, the changes are not so obvious. The further switching-off of the cw laser treatment leads to a slow decrease of the maxima and only after 21 h are these changes more prominent. The observed maxima are caused by photoinduced polarization of the corresponding trapping levels below the energy gap and it may indicate the occurrence of additional effective optical oscillators contributing to the effect. Such slow relaxation may be caused by depopulation of the corresponding metastable levels [26]. This is typical during photoinduced thermal effects [28].

Acknowledgements

For the author Ali Hussain Reshak this work was supported from the institutional research concept of the Institute of Physical Biology, UFB (No.MSM6007665808), the program RDI of the Czech Republic, the project CENAKVA (No. CZ.1.05/2.1.00/01.0024), the grant No. 152/2010/Z of the Grant Agency of the University of South Bohemia and the Institute of Nano Electronic Engineering, University Malaysia Perlis, 01000 Kangar, Perlis, Malaysia.

References

[1] Y.H. Lee, K.K. Chan, M.J. Brady, J. Vac. Sci. Technol. A 13 (1995) 596; W.C. Chen, Y.T. Wang, C.J. Shih, J. Alloys Compd. 490 (2010) 576.
[2] R. Malekfar, N. Mohammadian, S. Abbasian, F. Sadeghi, J. Alloys Compd. 488 (2009) 325; T. Nakayama, K. Onisawa, M. Fuyama, K. Hanazono, J. Electrochem. Soc. 139 (1992) 1204.
[3] K. Jurek, M. Guglielni, G. Kuncova, O. Renner, F. Lukes, M. Navratil, E. Krousky, V. Vorlicek, K. Kokesova, J. Mater. Sci. 27 (1992) 2549.
[4] F. Zhang, X. Liu, Y. Mao, N. Huang, Y. Chen, Z. Zheng, Z. Zhou, A. Chen, Z. Jiang, Surf. Coat. Technol. 103–104 (1998) 146.
[5] M. Gratzel, J. Photochem. Photobiol. C: Photochem. Rev. 4 (2003) 145.
[6] A.C. Van Popta, R.G. Decorby, C.J. Haugen, T. Robinson, J.N. Mcmullin, D. Tonchev, S.O. Kasap, Opt. Express. 10 (2002) 639.
[7] Q. Zhang, W. Liu, L. Liu, L. Xu, Y. Xu, G. Chen, Appl. Phys. Lett. 91 (2007) 181917.
[8] K. Shimakawa, Y. Ikeda, J. Optoelectron. Adv. Mater. 8 (2006) 2097.
[9] T. Wagner, M. Frumar, in: A.V. Kolobov (Ed.), Photo-Induced Metastability in Amorphous Semiconductors, Wiley, Germany, 2003, p. 160 (Chapter 10).
[10] D. Reyes-Coronado, G. Rodríguez-Gattorno, M.E. Espinosa-Pesqueira, C. Cab, R. de Coss, G. Oskam, Nanotechnology 19 (2008) 145605.
[11] P. Moriarty, Rep. Prog. Phys. 64 (2001) 297.
[12] K.M. Reddy, S.V. Manorama, A.R. Reddy, Mater. Chem. Phys. 78 (2003) 239.
[13] T. Guang-Lei, H. Hong-Bo, S. Jian-Da, Chin. Phys. Lett. 22 (2005) 1787.
[14] C. Ho, M.-C. Tsai, M.-S. Wong, Appl. Phys. Lett. 93 (2008) 081904.
[15] R. Asahi, Y. Taga, W. Mannstadt, A.J. Freeman, Phys. Rev. B 61 (2000) 7459; S. Kitazawa, S. Yamamoto, M. Asano, Y. Saitoh, S. Ishiyama, Nucl. Instrum. Methods Phys. Res. B 232 (2005) 94.
[16] E. Koścień, J. Sanetra, E. Gondek, B. Jarosz, I.V. Kityk, A.V. Kityk, Opt. Commun. 242 (2004) 401.
[17] I.V. Kityk, A. Kassiba, K. Plucinski, Phys. Lett. 265 (2000) 403.
[18] I.V. Kityk, M. Makowska-Janusik, A. Kassiba, Opt. Mater. 13 (2000) 449.
[19] E. Bertaud, International Tables for X-ray Crystallography, Kynoch Press, Birmingham, England, 1968, p. 318.
[20] M.K. Balakirev, I.V. Kityk, V.A. Smirnov, L.I. Vostrikova, J. Ebothe, Phys. Rev. A 67 (2003) 023806.
[21] T. Satyanarayana, I.V. Kityk, K. Ozga, M. Piasecki, P. Bragiel, M.G. Brik, V. Ravi Kumar, A.H. Reshak, N. Veeraiah, J. Alloys Compd. 482 (2009) 282.
[22] Y. Djaoued, S. Badilescu, P.V. Ashrit, D. Bersani, P.P. Lottici, R.J. Bruning, J. Sol–Gel Sci. Technol. 24 (2002) 247.
[23] S. Balaji, Y. Djaoued, J. Robichaud, J. Raman Spectrosc. 37 (2006) 1416.
[24] J. Tauc, Optical Properties of Solids, Academic Press, New York, 1966, pp. 277–313.
[25] A.G. Vedeshwar, J. Phys. III France 5 (1995) 1161.
[26] K.J. Plucinski, M. Makowska-Janusik, A. Mefleh, I.V. Kityk, V.G. Yushanin, Mater. Sci. Eng. B64 (1999) 88.
[27] H. Al-Dmour, D.M. Taylor, J.A. Cambridge, J. Phys. D: Appl. Phys. 40 (2007) 5034–5038.
[28] I.I. Syvorotka, V. Golub, I.M. Syworotka, J. Alloys Compd. 459 (2007) 487–490.